Reaction Kinetics, Mechanisms and Catalysis (2022) 135:1573–1586
https://doi.org/10.1007/s11144-022-02218-6

# Facile preparation of a Lewis acidic copper 1,3,5-benzenetricarboxylate with nanopore confinement superiority effect for enhanced catalytic Claisen-Schmidt condensation

**Nian Liu**[1] · **Ge Xu**[1]

Received: 8 January 2022 / Accepted: 30 March 2022 / Published online: 4 April 2022


## Abstract

Three copper 1,3,5-benzenetricarboxylate (Cu-BTC) samples were prepared by facile solvothermal methods in two mixed solvents (DMF/EtOH/$H_2O$ and EtOH/$H_2O$), and through steam-assisted conversion process (SAC). Furthermore, the physicochemical and spectroscopic analysis indicated the morphology, porosity and Lewis acidity of Cu-BTC samples could be easily changed by adjusting the kinds and amounts of solvents. The catalytic performance for synthesis of chalcone over three Cu-BTC samples was studied. It was found that Cu-BTC-STE shown a smaller acidic amount of 9.2 mmol/g, but presented the maximum yield of 84%, which was ascribed to its nanopore confinement superiority effect. Moreover, Cu-BTC-STE was easy for separation catalyst/product by the simple filtration and reused at least four recycles.

**Keywords** Cu-BTC · Inter-connective porous · Lewis acid · Heterogeneous catalyst · Chalcone · Pore confinement

## Introduction

Chalcone has gained increasing attention due to its significant applications, such as anti-inflammatory, anti-cancer [1–3]. Traditionally, synthesis method of chalcone is using the strong base or acid to catalyze Claisen-Schmidt condensation of acetophenone and benzaldehyde. The conventional catalysts for synthesis of chalcone include NaOH [4], KOH [5], HCl [6], and $H_3BO_3$ [7]. However, some obvious problems of these homogeneous catalytic reactions have been appeared in the industrial process:

✉ Ge Xu
gxu@sut.edu.cn

[1] School of Environment and Chemical Engineering, Shenyang University of Technology, Shenliao West Road 111, Economic & Technological Development Zone, 110870 Shenyang, People's Republic of China

disposable catalysts, large amounts of waste, and serious corrosion to equipment. For the past few years, various heterogeneous catalysts instead of homogeneous ones have been widely used to solve these problems, such as Zn-Al hydrotalcite [8], ZnO nanoflower [9] and metal organic framework (MOF) [10–13]. MOF is an intriguing porous hybrid material composed of metal atom as the center and organic ligand as the linker, which has excellent properties, including high specific surface area, stable reticular structure, adjustable pore sizes and much unsaturated active sites in the framework [14]. Cu-BTC MOF can be used as a favorite heterogeneous catalyst in a variety of organic reactions, such as Friedländer reaction of acetylacetone and 2-aminobenzophenone [15], Knoevenagel condensation of cyclohexaldehyde and benzaldehyde with active methylene compounds [16], Pechmann reaction of naphthol and ethyl acetoacetate [17]. Compared with Fe-BTC, ZIF-8, Zr-terephthalate MOF, and Alkaline earth metal-based MOF, Cu-BTC was found to be less efficient catalyst for the formation of chalcone [18]. It remains a challenge to enhance catalytic performance by controlling pore structure and active sites of Cu-BTC in order to be applied in chemical and pharmaceutical industry. For solvothermal and SAC methods, solvent environment can transfer electrons from unsaturated coordination metal to organic ligand in MOF framework [19], thus making MOF material with stronger Lewis acidity and more electronegative organic ligand. Lewis acidity of MOF material is not only significantly affected by solvent environment [20], but also whose geometrical structure can accurately manipulated by changing the kinds and amounts of solvents [21]. In addition to compare with solvothermal synthesis route, SAC synthesis has the advantages of gas–liquid reaction and less waste liquid, which is conducive to form more Lewis acidic sites and higher specific surface area [22].

In this work, three Cu-BTC MOFs were prepared by the solvothermal and SAC methods, in which the pore structure and acidic sites of the products can be manipulated by facile changing the kinds and amounts of solvents and removal of low-boiling solvents by vacuum drying. Moreover, the environment-friendly condensation of acetophenone and benzaldehyde was catalyzed by as-prepared three Cu-BTC samples. The catalytic results show that, the maximum yield of chalcone reached 84% using the octahedral Cu-BTC-STE with inter-connective nanopores as a catalyst. Cu-BTC catalysts were easy for separation catalyst/product by simple filtration and could suit requirements of industrialization. The yield of chalcone was calculated from weight of reactant and purified chalcone by filtering operation and recrystallization.

## Experimental section

### Materials

Copper (II) nitrate hydrate ($Cu(NO_3)_2{\cdot}3H_2O$, 99%), and benzene-1,3,5-tricarboxylic acid ($H_3BTC$, 98%) were purchased from Aladdin in China. Analytical grade solvents and other raw materials were purchased from Sinopharm Chemical Reagent Corp. (Shanghai, China) and used without further purification. Deionized

water was obtained from EasyQ-A10 Ultra-pure water system (JiZhou Chemical Technology Corp., China) in the laboratory.

### Facile preparation of Cu-BTC MOFs

In a typical solvothermal preparation, a solution of $Cu(NO_3)_2{\cdot}3H_2O$ (0.98 g) dissolved in deionized water (13.5 mL), and a solution of $H_3BTC$ (0.57 g) dissolved in ethanol (13.5 mL) were mixed together and stirred for 30 min. Then, the mixture are transferred into a Teflon-lined autoclave, and heated to 120 °C for 24 h in an oven. After naturally cooling down to room temperature, the product was washed with methanol for three times, then dried in an vacuum oven at 20 kPa, 60 °C for 12 h. As-obtained blue samples prepared in a DMF/EtOH/$H_2O$ solvent and an EtOH/$H_2O$ solvent were named as Cu-BTC-STD and Cu-BTC-STE.

Cu-BTC-SAC was synthesized by a SAC method (Scheme S1 in supplementary material). The mixed solvent (EtOH/$H_2O$, 1:1) was evenly poured into 45 g of zeolite, then the zeolite and the beaker containing $Cu(NO_3)_2{\cdot}3H_2O$ and $H_3BTC$ were sequentially transferred into the autoclave, especially the beaker was set above the zeolite. The other experimental steps of SAC were the same as that of solvothermal method. The synthesis conditions of Cu-BTC by the solvothermal and SAC methods were presented in Table 1.

**Table 1** Synthesis conditions of copper 1,3,5-benzenetricarboxylate samples prepared via solvothermal method in a DMF/EtOH/$H_2O$ solvent (Cu-BTC-STD), and solvothermal method in an EtOH/$H_2O$ solvent (Cu-BTC-STE), and steam-assisted conversion method (Cu-BTC-SAC)

| Sample | Cu-BTC-STD | Cu-BTC-STE | Cu-BTC-SAC |
|---|---|---|---|
| Metal atom source(A) | $Cu(NO_3)_2{\cdot}3H_2O$ | | |
| Organic ligand source(B) | $H_3BTC$ | | |
| Solvent for dissolving A(C) | Deionized water | | |
| Solvent for dissolving B(D) | 1:1 mixture of ethanol/DMF | Ethanol | Ethanol |
| Mole ratio A/B | 1.5 | | |
| mL of C | 20 | 13.5 | 2.5 |
| mL of D | 40 | 13.5 | 2.5 |
| Treatment before heating | Mixing and ultrasound for 10 min | Mixing and magnetically stirring the solution for 30 min | Full mixing |
| Reaction time(h) | 24 | | |
| Reaction temperature(°C) | 120 | | |
| Drying of filtered products | Drying in a vacuum oven at 20 kPa, 60 °C for 12 h | | |
| Appearance of products | Blue powder | | |
| Yield(%, based on $H_3BTC$) | 94 | 86 | 72 |

### Synthesis of chalcone

Cu-BTC catalyst (0.424 g, 4.7 wt%), acetophenone (4.6 mL), toluene (40 mL) mixed with sulfuric acid (1–2 drops) at 30 °C. Then, benzaldehyde (4.0 mL) was dropped into the mixture, and heated to 140 °C for 10 h. After the reaction was finished, the resulting solution and Cu-BTC catalyst were separated by the hot filtration. Then, the crude product was obtained by distilling the resulting solution at 180 °C under atmospheric pressure, and frozen for 12 h to collect the crystalline solid. Finally, the crystalline solid was recrystallized in ethanol and dried in vacuum oven at room temperature for 24 h, and weighed to calculate the yield.

### Characterizations

The surface morphology of Cu-BTC sample was acquired by using Hitachi SU8010 field emission scanning electron microscopy (FESEM). TEM images of the samples were obtained by the FEI TECNAI $G^2$ F30 transmission electron microscope with operating at an accelerating voltage of 300 kV. The Cu-BTC sample was ground into powder and collected for powder XRD characterization. Powder XRD patterns were collected by an Rigaku MiniFlex 600 diffractometer with Cu $K_\alpha$ radiation (40 kV, 15 mA, $\lambda = 1.54178$ Å). $N_2$ adsorption–desorption isotherms were obtained by the surface area and pore size distribution analyzer (JW-BK122W, JWGB Corp., China) after the samples were activated at 100 °C for 5 h. Temperature-programmed desorption of ammonia ($NH_3$-TPD) measurement was performed on a Micromeritic AutoChem II 2920 automatic adsorption instrument equipped with a thermal conductivity detector. The thermal stability of the sample was examined by the thermogravimetric analyzer (Q50, TA Instruments, USA) from room temperature to 700 °C under air flow.

The chalcone product by recrystallization purification was characterized by FTIR, NMR and HRMS (data shown in supplementary material). Direct transmittance was measured using KBr pellets on a Fourier transform spectrometer (IR Prestige-21, Shimadzu) in the range of 500–4000 $cm^{-1}$. $^1H$ NMR and $^{13}C$ NMR spectra were obtained by a Bruker AVANCE III 400 MHz digital nuclear magnetic resonance spectrometer with an internal standard of tetramethylsilane. High resolution MS was performed using Bruker apex-Ultra mass spectrometry.

## Results and discussion

### Characterization of inter-connective porous Cu-BTC

XRD curves of three Cu-BTC samples prepared by two solvothermal methods in different mixed solvents and SAC method are shown in Fig. 1. It is clearly seen that three samples indicate the same diffraction peaks and high crystallinity. The characteristic peaks of Cu-BTC MOF at $2\theta = 6.9°$, 9.5°, 11.7°, 13.6°, 14.9°, 16.5°,

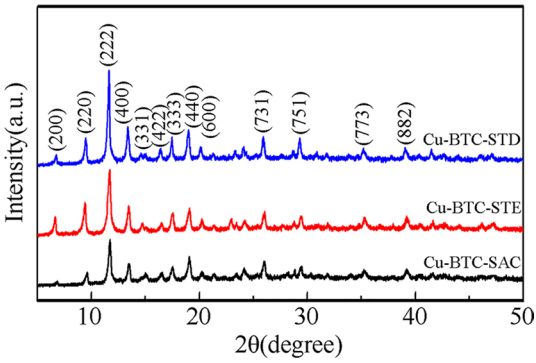


**Fig. 1** XRD curves of Cu-BTC samples prepared via solvothermal method in a DMF/EtOH/$H_2O$ solvent (Cu-BTC-STD), and solvothermal method in an EtOH/$H_2O$ solvent (Cu-BTC-STE), and steam-assisted conversion method (Cu-BTC-SAC)

17.5°, 18.9°, and 20.2° match well with the previously published data [23–25]. XRD results show that different preparations cause no apparent change of crystal structure, which suggest the framework structure of as-prepared Cu-BTC samples maintain stable.

The representative morphologies and particle sizes of as-prepared Cu-BTC MOFs were examined using SEM and TEM analysis. SEM image (Fig. 2a) of Cu-BTC-STD displays the irregular polyhedron shapes with size range of 5–10 μm, as well as the surfaces of Cu-BTC-STD are smooth with a few macro-pores and narrow stripes. In particular, Cu-BTC-STE sample (Fig. 2b) exhibits uniform octahedral

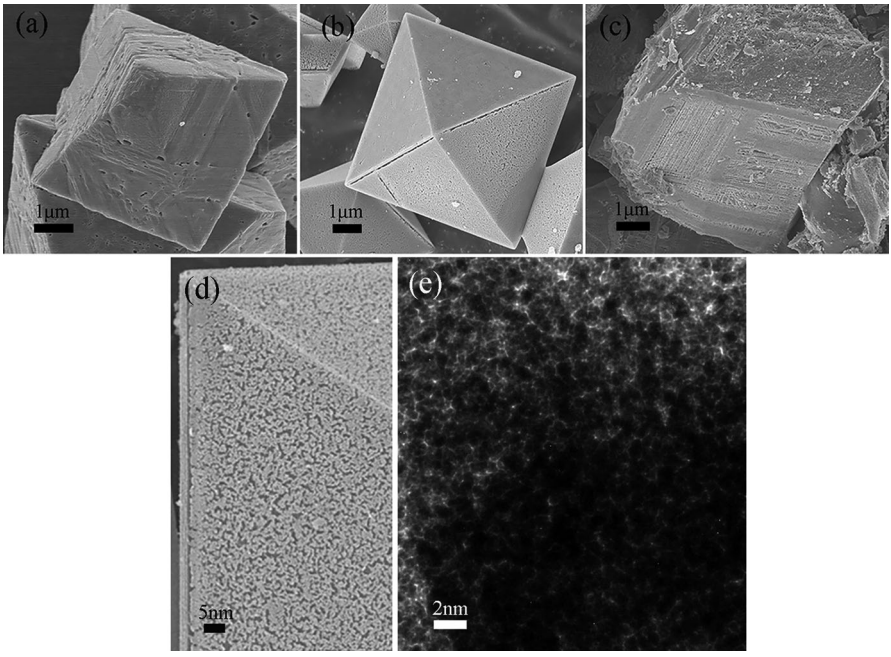


**Fig. 2** **a–c** SEM images of Cu-BTC-STD, STE and SAC; **d**, **e** Enlarged SEM, and TEM images of Cu-BTC-STE

morphology with well-distributed and cross-linked nanopores on the surfaces. The size of Cu-BTC-STE octahedrons in as-observed images range from about one to several micrometers. The SEM results illustrate that the products synthesized in the EtOH/$H_2O$ solvent environment (Fig. 2b) have better regularity of morphology than in the DMF/EtOH/$H_2O$ solvent environment (Fig. 2a). The difference between two solvent environments is that DMF is an aprotic polar solvent, while ethanol and water are the proton polar solvents. DMF can be converted to its corresponding amines at high temperatures and thus lead to deprotonation of organic linkers [19]. Here the difference in the solvent plays an important role in changing the morphology from irregular polyhedron to octahedron by affecting the bridging modes of ligand. SEM image of Cu-BTC-SAC (Fig. 2c) displays the morphology of irregular bulks with loose layers. The formation of loose layers are due to Cu-BTC-SAC products that were synthesized by the loss of solvent of crystallization [22]. As shown in Scheme S1, the steam formed by partial solvent evaporation promotes the reaction between metal ions and organic ligands. During this process, the solvents have been recycled completely and remained as little as possible in the framework. The particle sizes of Cu-BTC-SAC sample are about 5–10 microns. Microstructure of Cu-BTC-STE sample is examined exactly by high magnification SEM and TEM. From enlarge SEM image shown in Fig. 2d, it can be seen that the external surface of a typical Cu-BTC-STE sample is densely covered with cross-linked nanopores. From TEM image of the sample shown in Fig. 2e, the porous external surface of Cu-BTC-STE is formed by the nanopores, whose pore diameters are about 1–2 nm. The different contrast of the nanopores shown in Fig. 2e indicates that these nanopores have different pore depths resulted from the morphological characteristics of octahedron.

The porous and physical adsorption properties of Cu-BTC samples were verified by nitrogen adsorption–desorption isotherm measurements. As shown in Fig. 3a–c of $N_2$ adsorption–desorption isotherms of three Cu-BTC samples, the sharp increase of $N_2$ adsorption amount at relative pressure $P/P_0$ of around zero indicates that there are strong physical adsorption existing in Cu-BTC samples. In specially, the adsorption curve of Cu-BTC-STD (shown in Fig. 3a) increases rapidly at relative pressure $P/P_0$ ranged from 0.9 to 1.0, which confirms the existence of some macropores resulted from intra-agglomerate voids in the sample [26]. The curve of Cu-BTC-STE displays a type-I IUPAC isotherm (Fig. 3b), which are fully reversible as

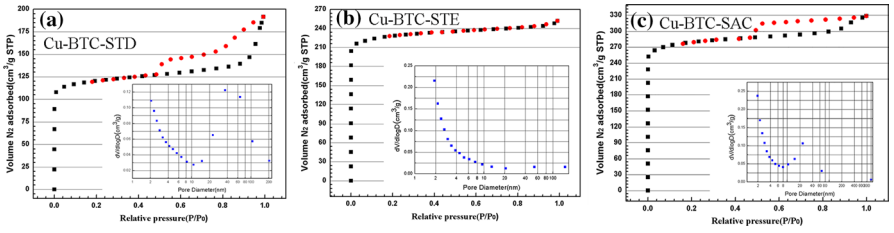


**Fig. 3** **a–c** $N_2$ adsorption–desorption isotherms of Cu-BTC-STD, STE and SAC; the markers representing pore size distribution of three Cu-BTC samples obtained by using the density functional theory are shown in the corresponding insets

indicated by the overlap of adsorption curves and desorption curves. The curve of Cu-BTC-SAC sample (shown in Fig. 3c) displays the H4 hysteresis loop which can be inferred that narrow slit pores formed by stacking of layered structures and slight crystal collapse happened during the solvent-evaporation process. Average pore diameters and specific surface areas of the samples were estimated with adsorption–desorption curve of isotherm by using DFT method (as exhibited in Table 2). The detailed pore size distribution of three Cu-BTC samples are shown in the insets of Fig. 3. The pore diameter distribution of Cu-BTC-STE (the inset of Fig. 3b) indicates that the distribution range is narrow and the size is within 2 nm. However, the distribution curves of the other two samples (the inset of Figs. 3a and c) indicate that their pores are consisted of a mixture of micropores and slit pores. The TEM and BET data indicate that Cu-BTC-STE sample has a nano-porous structure with excellent transparency, smooth pore wall, and uniform cross-sectional diameter of every pore. These results demonstrate that cross-linked nanopores not only exist on the external surface of Cu-BTC-STE (as shown in Fig. 2d and e), but also distribute into the interior of Cu-BTC-STE, forming an octahedral structure with inter-connective pores.

### Affirmations of Cu-BTC acidity and microstructure

Vibrational spectroscopy is one of valuable techniques for studying the molecular interactions between metal centers and organic ligands. FTIR spectra of as-prepared Cu-BTC samples were recorded as shown in Fig. S1. The characteristic peaks of unreacted $H_3BTC$ at around 760, 1100, 1372 and 1440 $cm^{-1}$ are observed for three samples, and the peak of all samples obtained at 728 $cm^{-1}$ may be due to the stretching modes of Cu–O. The results show that there are some identical chemical structures, including free organic acid ligands and reacted form of acid with Cu ions, in three Cu-BTC crystal structures. The strong absorption peaks at about 1560 and 1640 $cm^{-1}$ can be related to deprotonation of −COOH group in trimesic acid reacting with Cu ions [11], and C=O bond stretching in Cu-BTC. Infrared curves demonstrate that the stretching vibrations of C=O bond (1620 $cm^{-1}$) of Cu-BTC-STE shift to lower wavenumber as compared to Cu-BTC-SAC (1640 $cm^{-1}$), and then

**Table 2** Influence of porosity and acidity of as-prepared Cu-BTC catalysts on yield of chalcone

| Samples | Tm in $NH_3$-TPD-acidic amounts (mmol/g) | Surface area ($m^2$/g) | Average pore diameter (nm) | Density of acidic sites (mmol/$m^2$) | Yield of chalcone (%) | Y/aa |
|---|---|---|---|---|---|---|
| Cu-BTC-STD | 334 °C–10.3 | 413 | 2.9 | 0.025 | 58*/52** | 5.6* |
| Cu-BTC-STE | 325, 317 °C–9.2 | 818 | 1.9 | 0.011 | 84*/78** | 9.1* |
| Cu-BTC-SAC | 317 °C–24.5 | 987 | 2.1 | 0.025 | 71*/66** | 2.9* |

*Reaction conditions: catalyst (0.424 g), acetophenone (4.6 mL), sulfuric acid (1 ~ 2 drops), toluene (40 mL) and benzaldehyde (4.0 mL), 140 °C for 10 h

**Reaction conditions: other conditions are the same as above, without sulfuric acid

the absorption peak of coordinated –COOH group with Cu ions in Cu-BTC-SAC (1586 $cm^{-1}$) shift to higher wavenumber as compared to Cu-BTC-STE (1560 $cm^{-1}$). The results indicate that Cu-BTC-SAC with higher wavenumber has greater energy of coordinated –COOH group and C=O bond than Cu-BTC-STE base on the principle of infrared spectrum. But the existence of weak O–C=O absorption band (1700 $cm^{-1}$) in FTIR curve of Cu-BTC-STE shows that $H_3BTC$ complexing with the metal center has a novel mode. The formation of new O–C=O absorption band may be due to the organic linkers of Cu-BTC-STE accepting the electrons from the metal ions [27], which caused a novel electron-poor copper central ion with more Lewis acidic site.

$NH_3$-TPD characterization was carried out to affirm acidity of Cu-BTC catalysts. The $NH_3$-TPD profiles of three samples (Fig. S2 in supplementary material) show the obvious desorption signals at 250–350 °C, corresponding to strong Lewis acidic sites [28, 29]. The amounts of acid sites are associated with the peak areas of $NH_3$-TPD profiles, and the detailed data are listed in Table 2. It can be observed from $NH_3$-TPD desorption data, the total acid amounts followed the order Cu-BTC-SAC > Cu-BTC-STD > Cu-BTC-STE. The result demonstrated that added DMF can increases stability of unsaturated metal sites through deprotonation of organic linkers. As previously reported MOF materials [22, 23], the less solvent used and remained in the preparation can lead to faster crystallization rate and larger specific surface area. Because fewer solvents are used and remained in SAC process (as illustrated in Scheme S1 of supplementary material), Cu-BTC-SAC has higher surface areas of 987 $m^2/g$ than Cu-BTC-STD (413 $m^2/g$) and Cu-BTC-STE (818 $m^2/g$). Different from the other two curves in Fig. S2, the curve of Cu-BTC-STE shows two obvious $NH_3$ desorption peaks at 317 and 325 °C, indicating that the present of two Lewis acidic sites. According to reported simulation calculation data [27], two Lewis acidic sites in Cu-BTC-STE were derived from the unsaturated and novel electron-poor copper central ions. Considering the above infrared data, the $NH_3$-TPD results further prove that two types of copper acidic sites are formed in Cu-BTC-STE sample.

The thermal stability of Cu-BTC material is helpful for precise understanding the property of surface acidity, solvent residues and framework construction. Hence the thermal decomposition curves of three Cu-BTC samples under air atmosphere using thermogravimetric (TG) analyzer are shown in Fig. 4. By comparison of three TG signals, it's obvious that the curve of Cu-BTC-SAC sample shows a significant difference. The first weight loss (about 17%) of Cu-BTC-SAC terminated at 125 °C is due to the vaporization of solvent residues inside the framework whereas the second weight loss (about 7%) up to 319 °C can attributed to removal of guest molecules from open metal sites on Cu-BTC-SAC surfaces. The TGA curve of Cu-BTC-SAC containing slow second-step weight reduction is the typical characteristic of a MOF material having open metal sites [30]. After further heating, the final major weight loss (about 35%) was observed within 319–385 °C for Cu-BTC-SAC, indicating that the catalyst is thermally stable up to 319 °C. Because using similar synthetic methods and solvents, Cu-BTC-STE and Cu-BTC-STD samples were able to identify similar weight loss stages in their TG curves. The first weight loss (about 5%) up to 150 °C was ascribed to the removal of solvent residues in Cu-BTC-STE or

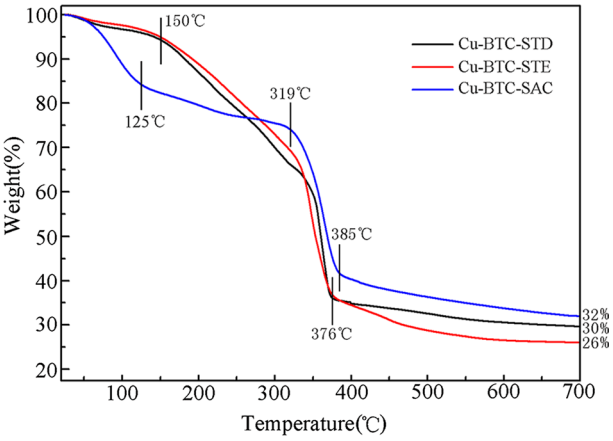


**Fig. 4** Thermogravimetric analysis curves of Cu-BTC-STD, STE and SAC

Cu-BTC-STD. The second TG step with large mass loss (about 60%) in 150–376 °C region was related to the thermal decomposition and combustion of organic ligands from the interior of framework. The destruction of organic ligands indicates that corresponding metal sites of Cu-BTC-STE and Cu-BTC-STD samples aren't on the surfaces. The TG curves of Cu-BTC-STD and Cu-BTC-STE displayed the slight decrease above 376 °C, which could be explained for a complete transformation into carbide and oxide of copper. Cu-BTC-STE and Cu-BTC-STD samples ultimately showed the continuous mass loss of 26% and 30% up to temperature of 700 °C.

Through judicious choice of prepared method, Cu-BTC MOF materials with inter-connective nanopores can be synthesized. The morphology, pore sizes, acidity of these porous MOFs can be easily tuned by controlling kinds and amounts of solvents, and removal of partial solvents in the solvothermal or SAC synthesis. In specially, an effective post-processing method has been employed, which is using low boiling methanol to replace and remove small molecular solvents in the framework through vacuum drying. It is clear that Cu-BTC-STE could expose two types of Lewis acidic sites that may originate from the activity of copper central ion in the proton solvent and the replacement of ethanol with methanol. For Cu-BTC-STD sample, it cannot be completely replaced to form a novel Cu acid center due to the deprotonation of DMF, but it helps to produce more acidity. Cu-BTC-SAC sample with open metal sites has the highest acidic amount because of open metal sites mean more unsaturated central ions.

## Catalytic synthesis of chalcone

The Cu-BTC samples were chosen as an acidic solid catalyst for the Claisen-Schmidt condensation of acetophenone and benzaldehyde to yield chalcone (characterization data in Figs. S3–S7). As listed in Table 2, the reaction occurred readily to give 58% yield of chalcone using Cu-BTC-STD catalyst, while yields of 84% and 71% were observed using Cu-BTC-STE and Cu-BTC-SAC catalysts, respectively.

In order to confirm the effect of sulfuric acid on catalysis the controlled experiments were performed. The yield of 78% for synthesis of chalcone can be obtained through catalyzing by Cu-BTC-STE without sulfuric acid, and the data has been added to Table 2. The catalytic effect of sulfuric acid on chalcone is rarely reported [31], but sulfuric acid modified silica [32] and fly-ash [33] solid catalysts may catalyze the synthesis of chalcone. Sulfuric acid can be used as an activator for the Cu-BTC catalyst and promote the reaction.

Because sulfuric acid has the same activation effect on three catalysts (displayed in Table 2), it should be noted that chalcone catalyzed by Cu-BTC-STE demonstrated lower Lewis acidity than Cu-BTC-SAC and Cu-BTC-STD. In the process of acid catalyzed synthesis of chalcone, the carbonyl of benzaldehyde is firstly activated by acidic sites and then forms a nucleophilic α-C. This activation occurs when the distance between acidic sites and the carbonyl of benzaldehyde is shortened to a certain extent. Therefore, shortening the distance between active sites and reactants become the key control factor. As a result, the higher catalytic activity of Cu-BTC-STE sample could be associated with its inter-connective pores (Figs. 2 and 3). The nanopores (average pore diameter 1.9 nm) of octahedral Cu-BTC-STE are accessible for the reactants of acetophenone and benzaldehyde (single molecular diameter about 0.7 nm), which thus can be activated on the acidic sites located on the internal pore wall. In order to further explain the relationship between acid amount, specific surface area and yield of chalcone, two new parameters are introduced. The density of acidic sites is the ratio of acidic amounts and surface area, and the Y/aa is the ratio of yield of chalcone and acidic amounts. As shown in Table 2, the density of acidic sites of Cu-BTC-STE is lower than Cu-BTC-STD and Cu-BTC-SAC, but it get the highest Y/aa. The amount of acidic sites is not the key to the catalytic activity, but enhanced catalytic effect can be produced when the acid sites are close to the reactants. Compared with Cu-BTC-STD and Cu-BTC-SAC, Cu-BTC-STE sample has inter-connective pores within 2 nm size which can promote the active sites reacting with the reactants.

Base on the above analysis, potential synthesis mechanism of chalcone with Cu-BTC-STE as a catalyst is proposed (as shown in Fig. 5). Firstly, the carbonyl of benzaldehyde is activated by two types of copper Lewis acidic sites, and then coordinated with which facilitates the reaction with α-C of nucleophilic reagent acetophenone to form β-hydroxy ketone. Finally β-hydroxy ketone is dehydrated to produce the chalcone. Excellent catalytic performance of Cu-BTC-STE resulted in its uniform nanopores with excellent transparency and two types of internal cooper Lewis acidic sites. Above these results indicated that the catalytic performance of Cu-BTC-STE was defined as the nanopore confinement superiority effect.

Compared with zeolite [34–36], carbon nanotube [37] and $MoO_3$-$Al_2O_3$ [38] catalysts, there is no report that MOF materials with pore confinement effect. The heterogeneous catalyst reusability and stability of catalytic activity play a significant role in the industrial application. Thus, the recycling experiment of Cu-BTC-STE catalyst was carried out at optimized conditions. After each reaction, Cu-BTC-STE catalyst was hot filtered off, washed and dried under vacuum at room temperature for 1 h, and reused for next run without further treatment. As demonstrated in Fig. S8 of supplementary material, Cu-BTC-STE catalyst reused at least four recycles

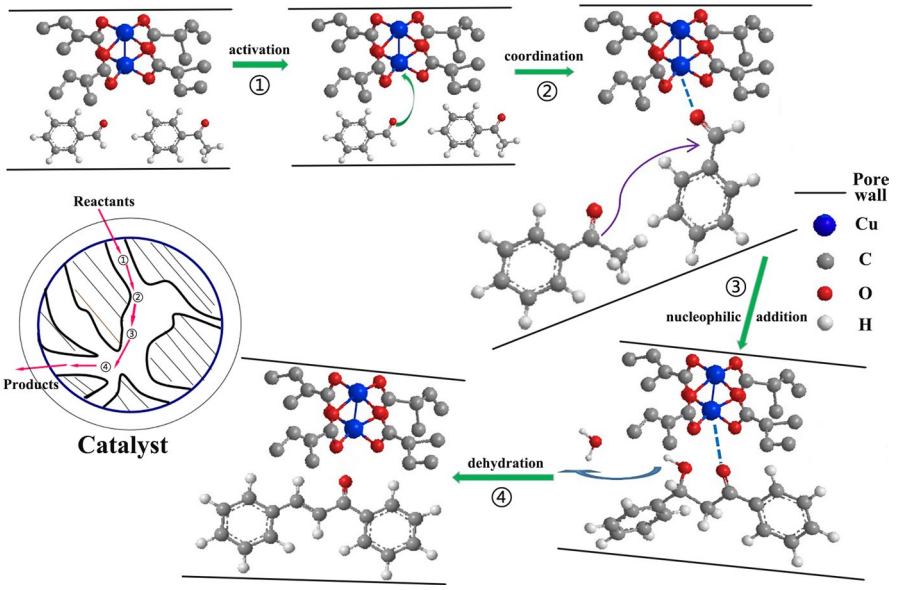


**Fig. 5** Proposal synthesis mechanism of chalcone catalyzed by Cu-BTC-STE with nanopore confinement superiority effect

with average 1.25% decrease in yields per cycle. It provides a new idea for constructing more durable MOF heterogeneous catalysts and a suitable mean of their recovery, reactivation [39].

## Conclusions

In this research, Cu-BTC MOFs were prepared by the facile solvothermal and SAC methods, and then characterized by XRD, SEM, TEM, BET, TGA, $NH_3$-TPD and FTIR measurements. The results reveal the octahedral Cu-BTC-STE with inter-connective nanopores and internal double Lewis acidic sites. In addition, it has been shown that as-prepared Cu-BTC samples can efficiently catalyze the synthesis of chalcone. Using Cu-BTC-STE as a heterogeneous catalyst, the maximum yield of 84% was obtained. Compared to Cu-BTC-STD and Cu-BTC-SAC catalysts, Cu-BTC-STE catalyst had a higher activity due to confinement superiority effect produced by inter-connective nanopores. This achievement would contribute to the development of porous Cu-BTC MOFs as the high selectivity heterogeneous catalysts, which would be an industrially viable and sustainable alternative to other solid catalysts for synthesis of organic compound.

**Supplementary Information** The online version contains supplementary material available at https://doi.org/10.1007/s11144-022-02218-6.

**Funding** This work was supported by Scientific Research Project of Liaoning Provincial Education Department (No. LJKZ0155).

## Declarations

**Conflict of interest** The authors have no competing interest to declare that are relevant to the content of this article.

## References


1. Yang HM, Shin HR, Cho SH, Bang SC, Song GY, Ju JH, Kim MK, Lee SH, Ryu JC, Kim YS, Jung SH (2007) Structural requirement of chalcones for the inhibitory activity of interleukin-5. Bio Medic Chem 15(1):104–111. https://doi.org/10.1016/j.bmc.2006.10.007
2. Bandgar BP, Gawande SS, Bodade RG, Totre JV, Khobragade CN (2010) Synthesis and biological evaluation of simple methoxylated chalcones as anticancer, anti-inflammatory and antioxidant agents. Bio Medic Chem 18(3):1364–1370. https://doi.org/10.1016/j.bmc.2009.11.066
3. Bondock S, Naser T, Ammar YA (2013) Synthesis of some new 2-(3-pyridyl)-4,5-disubstituted thiazoles as potent antimicrobial agents. Eur J Medic Chem 62:270–279. https://doi.org/10.1016/j.ejmech.2012.12.050
4. Domínguez JN, Charris JE, Lobo G, de Domínguez NG, Moreno MM, Riggione F, Sanchez E, Olson J, Rosenthal PJ (2001) Synthesis of quinolinyl chalcones and evaluation of their antimalarial activity. Eur J Medic Chem 36(6):555–560. https://doi.org/10.1016/s0223-5234(01)01245-4
5. Yao NH, Song AM, Wang XB, Dixon S, Lam KS (2007) Synthesis of flavonoid analogues as scaffolds for natural product-based combinatorial libraries. J Comb Chem 4:668–676. https://doi.org/10.1021/cc070009y
6. Aichaoui H, Guenadil F, Kapanda CN, Lambert DM, McCurdy CR, Poupaert JH (2009) Synthesis and pharmacological evaluation of antioxidant chalcone derivatives of 2(3H)-benzoxazolones. Med Chem Res 18(6):467–476. https://doi.org/10.1007/s00044-008-9143-y
7. Zhang XW, Zhao DH, Quan YC, Sun LP, Yin XM, Guan LP (2010) Synthesis and evaluation of antiinflammatory activity of substituted chalcone derivatives. Med Chem Res 19(4):403–412. https://doi.org/10.1007/s00044-009-9202-z
8. Kunde LB, Gade SM, Kalyani VS, Gupte SP (2009) Catalytic synthesis of chalcone and flavanone using Zn–Al hydrotalcite adhere ionic liquid. Catal Comm 10(14):1881–1888. https://doi.org/10.1016/j.catcom.2009.06.018
9. Tamuly C, Saikia I, Hazarika M, Bordoloi M, Hussain N, Das RM (2015) Bio-derived ZnO nanoflower: a highly efficient catalyst for synthesis of chalcones derivatives. RSC Adv 5(12):8604–8608. https://doi.org/10.1039/c4ra14225j
10. Corma A, García H, Llabrés i Xamena FX (2010) Engineering metal organic frameworks for heterogeneous catalysis. Chem Rev 110(8):4606–4655. https://doi.org/10.1021/cr9003924
11. Wu SH, Ma X, Ran JY, Zhang YF, Qin FX, Liu Y (2015) Application of basic isoreticular nanoporous metal-organic framework: IRMOF-3 as a suitable and efficient catalyst for the synthesis of chalcone. RSC Adv 5(19):14221–14227. https://doi.org/10.1039/c4ra16180g
12. Jiang HX, Wang ST, Wang CX, Chen YF, Zhang MH (2018) Selective catalytic reduction of $NO_x$ with $NH_3$ on Cu-BTC-derived catalysts: influence of modulation and thermal treatment. Catal Surv Asia 22:95–104. https://doi.org/10.1007/s10563-018-9242-9
13. Nguyen LTL, Nguyen TT, Nguyen KD, Phan NTS (2012) Metal-organic framework MOF-199 as an efficient heterogeneous catalyst for the aza-Michael reaction. Appl Catal A 425–426:44–52. https://doi.org/10.1016/j.apcata.2012.02.045
14. Janiak C, Vieth JK (2010) MOFs, MILs and more: concepts, properties and applications for porous coordination networks (PCNs). New J Chem 34(11):2366–2388. https://doi.org/10.1039/c0nj00275e
15. Pérez-Mayoral E, Čejka J (2011) $[Cu_3(BTC)_2]$: a metal-organic framework catalyst for the Friedländer reaction. ChemCatChem 3(1):157–159. https://doi.org/10.1002/cctc.201000201
16. Opanasenko M, Dhakshinamoorthy A, Shamzhy M, Nachtigall P, Horáček M, Garcia H, Čejka J (2013) Comparison of the catalytic activity of MOFs and zeolites in Knoevenagel condensation. Catal Sci Technol 3(2):500–507. https://doi.org/10.1039/c2cy20586f
17. Opanasenko M, Shamzhy M, Čejka J (2012) Solid acid catalysts for coumarin synthesis by the pechmann reaction: MOFs versus Zeolites. ChemCatChem 5(4):1024–1031. https://doi.org/10.1002/cctc.201200232

18. Panchenko VN, Timofeeva MN, Jhung SH (2016) Metal-organic frameworks with Lewis acidity: synthesis, characterization, and catalytic applications. Catal Rev 58(2):209–307. https://doi.org/10.1080/01614940.2016.1128193
19. Seetharaj R, Vandana PV, Arya P, Mathew S (2019) Dependence of solvents, pH, molar ratio and temperature in tuning metal organic framework architecture. Arab J Chem 12:295–315. https://doi.org/10.1016/j.arabjc.2016.01.003
20. DeCoste JB, Peterson GW, Schindler BJ, Killops KL, Broweb MA, Mahle JJ (2013) The effect of water adsorption on the structure of the carboxylate containing metal-organic frameworks Cu-BTC, Mg-MOF-74, and UiO-66. J Mater Chem A 1(38):11922–11932. https://doi.org/10.1039/C3TA12497E
21. Yu DB, Shao Q, Song QJ, Cui JW, Zhang YL, Wu B, Ge L, Wang Y, Zhang Y, Qin YQ, Vajtai R, Ajayan PM, Wang HT, Xu TW, Wu YC (2020) A solvent-assisted ligand exchange approach enables metal-organic frameworks with diverse and complex architectures. Nature Comm 11(1):927. https://doi.org/10.1038/s41467-020-14671-9
22. Chen Y, Yang CY, Wang XQ, Yang JF, Li JP (2016) Vapor phase solvents loaded in zeolite as the sustainable medium for the preparation of Cu-BTC and ZIF-8. Chem Eng J 313:179–186. https://doi.org/10.1016/j.cej.2016.12.055
23. Yang Y, Shukla P, Wang SB, Rudolph V, Chen XM, Zhu ZH (2013) Significant improvement of surface area and $CO_2$ adsorption of Cu–BTC via solvent exchange activation. RSC Adv 3(38):17065–17072. https://doi.org/10.1039/c3ra42519c
24. Yang YQ, Dong H, Wang Y, He C, Wang YX, Zhang XD (2018) Synthesis of octahedral like Cu-BTC derivatives derived from MOF calcined under different atmosphere for application in CO oxidation. J Solid State Chemistry 258:582–587. https://doi.org/10.1016/j.jssc.2017.11.033
25. Nobar SN (2018) Cu-BTC Synthesis, characterization and preparation for adsorption studies. Mater Chem Phys 213:343–351. https://doi.org/10.1016/j.matchemphys.2018.04.031
26. Kim KJ, Li YJ, Kreider PB, Chang CH, Wannenmacher N, Thallapally PK, Ahn HG (2013) High-rate synthesis of Cu-BTC metal-organic frameworks. Chem Commun 49:11518. https://doi.org/10.1039/c3cc46049e
27. Rubeš M, Grajciar L, Bludský O, Wiersum AD, Llewellyn PL, Nachtigall P (2012) Combined theoretical and experimental investigation of CO adsorption on coordinatively unsaturated sites in CuBTC MOF. ChemPhysChem 13(2):488–495. https://doi.org/10.1002/cphc.201100602
28. Zhang YK, Ding CM, Wang JW, Jia YM, Xue YA, Gao ZT, Yu B, Gao BZ, Zhang K, Liu P (2019) Intermediate product regulation over tandem catalysts for one-pass conversion of syngas to ethanol. Catal Sci Technol 9(7):1581–1594. https://doi.org/10.1039/c8cy02593b
29. Zhang Y, Chen T, Zhang G, Wang GY, Zhang H (2018) Mesoporous Al-promoted sulfated zirconia as an efficient heterogeneous catalyst to synthesize isosorbide from sorbitol. Appl Catal A 562:258–266. https://doi.org/10.1016/j.apcata.2018.06.024
30. Feng C, Cao XL, Zhang LG, Guo CY, Akram N, Wang JD (2018) Zn 1,3,5-benzenetricarboxylate as an efficient catalyst for the synthesis of cyclic carbonates from $CO_2$. RSC Adv 8(17):9192–9201. https://doi.org/10.1039/c8ra00152a
31. Bukhari SNA, Jasamai M, Jantan I, Ahmad W (2013) Review of methods and various catalysts used for chalcone synthesis. Mini-Rev Org Chem 10:73–83. https://doi.org/10.2174/1570193X11310010006
32. Sultan A, Raza AR, Abbas M, Khan KM, Tahir MN, Saari N (2013) Evaluation of silica-$H_2SO_4$ as an efficient heterogeneous catalyst for the synthesis of chalcones. Molecules 18:10081–10094. https://doi.org/10.3390/molecules180810081
33. Thirunarayanan G, Mayavel P, Thirumurthy K (2012) Fly-ash:$H_2SO_4$ catalyzed solvent free efficient synthesis of some aryl chalcones under microwave irradiation. Spectrochimica Acta Part A 91:18–22. https://doi.org/10.1016/j.saa.2012.01.054
34. Di Iorio JR, Johnson BA, Román-Leshkov Y (2020) Ordered hydrogen-bonded alcohol networks confined in Lewis acid zeolites accelerate transfer hydrogenation turnover rates. J Am Chem Soc 142(45):19379–19392. https://doi.org/10.1021/jacs.0c09825
35. Palčić A, Valtchev V (2020) Analysis and control of acid sites in zeolites. Appl Catal A 606:1–32. https://doi.org/10.1016/j.apcata.2020.117795
36. Jones AJ, Zones SI, Iglesia E (2014) Implications of transition state confinement within small voids for acid catalysis. J Phys Chem C 118(31):17787–17800. https://doi.org/10.1021/jp5050095

37. Wei X, Zhang YH, Liew KY, Li JL (2012) Effect of catalyst confinement and pore size on Fischer-Tropsch synthesis over cobalt supported on carbon nanotubes. Sci China Chem 55:1811–1818. https://doi.org/10.1007/s11426-012-4727-2
38. Zhang D, Liu WQ, Liu YA, Etim UJ, Liu XM, Yan ZF (2017) Pore confinement effect of $MoO_3$/$Al_2O_3$ catalyst for deep hydrodesulfurization. Chem Eng J 330:706–717. https://doi.org/10.1016/j.cej.2017.08.02
39. Molnár Á, Papp A (2017) Catalyst recycling-a survey of recent progress and current status. Coord Chem Rev 349:1–65. https://doi.org/10.1016/j.ccr.2017.08.011